Chemical Science

ROYAL SOCIETY OF CHEMISTRY

EDGE ARTICLE

View Article Online
View Journal | View Issue

Cite this: *Chem. Sci.*, 2022, **13**, 9381

All publication charges for this article have been paid for by the Royal Society of Chemistry

Received 13th May 2022
Accepted 18th July 2022

DOI: 10.1039/d2sc02662g

rsc.li/chemical-science

Green-/NIR-light-controlled rapid photochromism featuring reversible thermally activated delayed fluorescence and photoelectronic switching†

Ziyong Li, Ji-Rui Zhang, Xu-Ke Tian, Shuren Yang, Si Chen, Hui Zhou and Xiao-Gang Yang *

Fluorescent dithienylethene-based photochromic materials have been attracting considerable attention owing to their wide applications in biological and materials sciences. However, the limitations of detrimental UV irradiation for photocyclization, short emission lifetime, and inefficient photoresponsive speed still need to be addressed. Herein, a novel dithienylethene photochromic molecule, **BFBDTE**, has been prepared by the incorporation of a difluoroboron β-diketonate (BF_2bdk) unit. The strong electron acceptor BF_2bdk not only reduces the energy gap of the open isomer, ensuring visible light-controlled fluorescence switching, but also promotes intersystem crossing for the generation of thermally activated delayed fluorescence (TADF). Upon alternating irradiation with green and NIR light, **BFBDTE** presents a rare example of photochromism, fluorescence and TADF switching in various polar solvents and a poly(methyl methacrylate) (PMMA) film. Meanwhile, it shows rapid and well repeatable cyclization (12 s) and cycloreversion reactions (20 s) in PMMA, accompanied by fast TADF switching within 11 s. Furthermore, photo-electrochemical measurements reveal a remarkable on-off photoelectronic response (photocurrent density ratio: I_{light}/I_{dark} = 684) between the open- and closed-form of **BFBDTE**. These remarkable merits make **BFBDTE** promising for photoswitchable molecular devices, optical memory storage systems, NIR detectors, and photoelectric switching.

Introduction

Photochromic fluorescence switches, whose emission can be reversibly switched *via* light irradiation, have recently aroused tremendous attention due to their potential in optoelectronic materials, bioimaging and super-resolution microscopy.[1–6] As a core structural motif of a photochromic switch, the reversible cyclization/cycloreversion of dithienylethenes (DTEs) upon light irradiation has continued to attract substantial scientific interest.[7] Recently, the combination of DTE photoswitching and a fluorescent unit has become a kind of appealing fluorescence switch arising from their thermo-stability, robust fatigue resistance and rapid response.[8–11] A general scheme for designing such switches is a dyad system comprising one fluorophore and DTE unit in the same molecule, facilitating fluorescence quenching through intramolecular energy transfer (ET).[12] As depicted in Scheme 1a, the ring-open state of DTE with high S_1 energy restrains the energy transfer from the excited fluorophore to the open isomer, retaining the fluorescence emission of the fluorophore. Upon irradiation with UV light, the ring-closed state with low S_1 energy enables energy transfer, and then quenches the fluorescence emission. Although great progress has been made in fluorescence switches in recent years,[13–18] they still suffer from several drawbacks, *e.g.*, the necessity of UV light to switch the fluorescence emission, inferior photoresponsive speed (several minutes), and short fluorescence lifetimes. Considering the high phototoxicity and low penetrability of UV light, numerous efforts have been devoted to fabricating visible light-activated fluorescence switches, of which simply extending the π-conjugation length by connecting aromatic fluorescent dyes on the peripheral thienyls of DTE is most appealing.[19–25] However, the slow photoresponsive speed and short fluorescence lifetime with a time scale of nanoseconds (τ < 10 ns) still limit their further applications.

Fortunately, a novel class of fluorophores with long fluorescence lifetimes, *i.e.*, thermally activated delayed fluorescence (TADF),[26–28] may provide a possible solution to the above issues. As illustrated in Scheme 1b, the TADF process can undergo efficient ISC and then reverse intersystem crossing (RISC) for 100% internal quantum efficiency from T_1 to S_1 due to a remarkably small energy gap (ΔE_{ST} < 0.2 eV) between the lowest singlet excited states and the lowest triplet excited states, which makes them promising candidates for various applications in organic light-emitting diodes (OLEDs), triplet–triplet

College of Chemistry and Chemical Engineering, College of Food and Drug, Luoyang Normal University, Luoyang 471934, P. R. China. E-mail: yxg2233@126.com

† Electronic supplementary information (ESI) available. CCDC 2171748. For ESI and crystallographic data in CIF or other electronic format see https://doi.org/10.1039/d2sc02662g

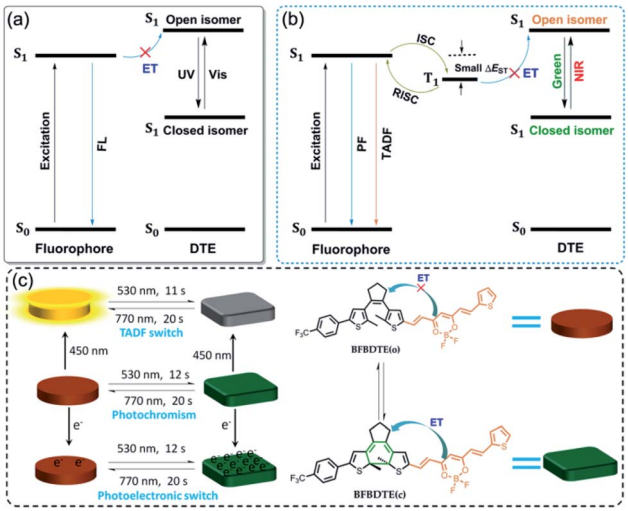

Scheme 1 (a) Schematic illustrations of the energy transfer process upon UV and visible light irradiation in traditional photochromic fluorescence switching. (b) Proposed schematic illustrations of photochromic TADF switching. (c) Green-/NIR-light-controlled rapid photochromism featuring reversible TADF and photoelectronic switching. FL: fluorescence, PF: prompt fluorescence, TADF: thermally activated delayed fluorescence, S_0: ground state, S_1: excited singlet state, T_1: excited triplet state, ET: energy transfer, ISC: intersystem crossing, RISC: reverse intersystem crossing, ΔE_{ST}: singlet–triplet energy gap.

annihilation upconversion (TTA-UC), time-resolved fluorescence imaging (TRFI), photodynamic therapy (PDT) and organic photocatalytic synthesis.[29–31] Inspired by the desired fluorescence efficiencies and lifetimes of TADF, we speculate that the incorporation of the TADF process into visible light-driven DTE systems could obviously improve the photoswitching efficiencies applied in photoswitchable molecular devices, optical memory storage systems and bioimaging with deeper light penetration. So far, only one example of TADF-based photochromic switching has been reported.[32] Therefore, developing efficient visible light-controlled DTE systems with multi-mode TADF characteristics is highly desirable for photoelectric applications, but remains a severe challenge.

To prove our hypothesis, a novel DTE molecular switch modified by a difluoroboron β-diketonate (BF_2bdk) moiety has been successfully prepared (Scheme 1c), in which the incorporation of active nonbonding p electrons on the BF_2bdk group promotes the spin-orbital coupling (SOC) between the excited singlet and triplet states in favor of enhanced intersystem crossing (ISC).[33] Moreover, the strong electron acceptor BF_2bdk can bring about intramolecular charge transfer (ICT), which endows a typical TADF feature with small ΔE_{ST} for efficient ISC and RISC processes.[34] On the other hand, merging BF_2bdk and DTE can not only extend the π-conjugation, but also reduce the HOMO–LUMO energy gap of the open isomer, which will ensure excellent visible light-controlled fluorescence switching with high photoresponsive speed.[35] As expected, the obtained fluorescent DTE (**BFBDTE**) shows rapid and long-term reversible tri-channels of photochromism, fluorescence and TADF switching in toluene and a poly(methyl methacrylate) (PMMA) film. It represents the first example of green-/NIR-light-controlled photoswitching with the combination of photochromism and TADF.

Results and discussion

As depicted in Scheme S1,† **BFBDTE** was prepared by the Knoevenagel condensation reaction between intermediates 4 and 5 under the catalysis of *n*-butylamine in anhydrous toluene in a yield of 69%. Its chemical structure was characterized by NMR spectroscopy, high-resolution mass spectrometry (Fig. S1–S3†) and single-crystal X-ray diffraction. From its ^{1}H NMR spectrum, the coupling constants of the vinyl double bonds were 15.0 or 15.2 Hz, respectively, revealing the usual *trans*-configuration for both ethylene bonds in **BFBDTE**. An orange-red crystal was isolated by the slow volatilization of its chloroform solution. Single-crystal X-ray diffraction analysis reveals that **BFBDTE** crystallizes in the triclinic $P\bar{1}$ space group (Table S1†). As depicted in Fig. 1a, **BFBDTE** presents an antiparallel conformation where the distance between the two reactive carbon atoms was as short as 3.57 Å (<4.2 Å), indicating that the photocyclization was easy to access.[36] The **BFBDTE** molecules are linked together by C–H···F hydrogen bonding interactions giving rise to a 1D chain running along the *a* direction (Fig. 1b, S4 and S5†). Herein, the hydrogen bonding acceptors are all from the F atoms of difluoroboron. As shown in Fig. S6,† each chain is further extended to a 2D layer and then a 3D structure through C–H···F halogen bonding interactions with $-CF_3$ as a hydrogen bonding acceptor. Viewed along the *a* direction, the packing structure exhibits an alternant arrangement of BF_2bdk and DTE at the molecular level.

The photochromism of **BFBDTE** was then investigated in different polar solvents. As illustrated in Fig. 2a, it was clear that two absorption bands of the open isomer **BFBDTE(o)** centered

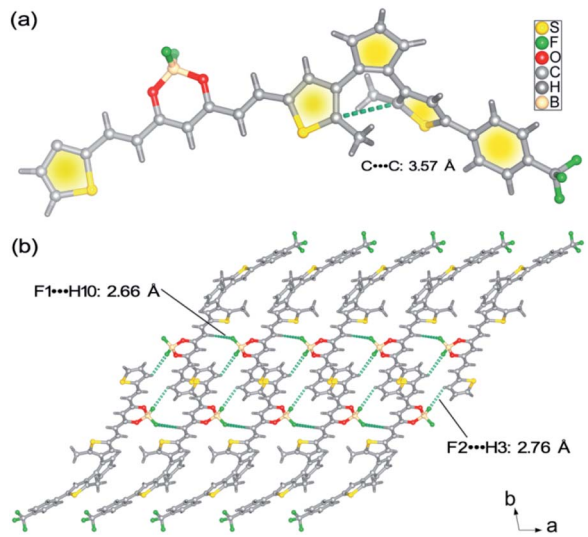

Fig. 1 (a) Crystal structure of the **BFBDTE** molecule. (b) View of the 1D chain structure of **BFBDTE** extended by C–H···F hydrogen bonding.

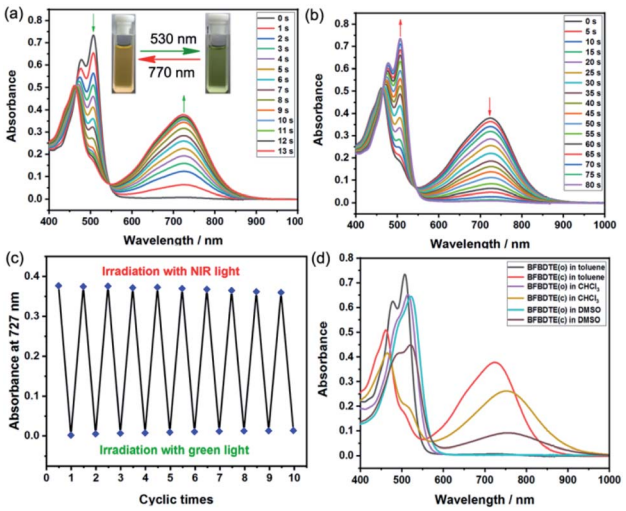

Fig. 2 The absorption spectra changes of **BFBDTE** in toluene (2.0×10^{-5} mol L^{-1}) upon alternating irradiation with green light at 530 nm (a) and NIR light at 770 nm. (b) The insets show the corresponding color changes upon photoirradiation. (c) The fatigue resistance of **BFBDTE** in toluene for ten cycles. (d) The absorption spectra of **BFBDTE** before and after irradiation with green light in various solvents (2.0×10^{-5} mol L^{-1}).

at 478 nm ($\varepsilon = 3.12 \times 10^4$ M^{-1} cm^{-1}) and 509 nm ($\varepsilon = 3.68 \times 10^4$ M^{-1} cm^{-1}) were observed in toluene, which are derived from the intramolecular charge transfer (ICT) transition.[37] Upon green-light irradiation (530 nm), a near-infrared absorption band centered at 727 nm ($\varepsilon = 1.88 \times 10^4$ M^{-1} cm^{-1}) gradually emerged along with the color changing from orange-yellow to green (Fig. 2a, insets), indicating the formation of the ring-closed isomer **BFBDTE(c)** (Scheme 1c). It is worth noting that the achievement of the photostationary state only takes 13 s of green-light irradiation. The response rate for **BFBDTE** is faster than that of the reported Pt-DTE (120 s)[38a] and POM-DTE complexes (65 min)[38b] detected in organic solvents. Moreover, an isosbestic point at 546 nm was observed, clearly indicating the photochromic transformation between **BFBDTE(o)** and **BFBDTE(c)**. Irradiation with NIR light ($\lambda = 770$ nm, 80 s) triggered the cycloreversion reaction to regenerate the initial orange-yellow isomer (Fig. 2b). Further fatigue resistance results indicated good reversibility (without obvious degradation for ten cycles) between the open and closed forms under green/NIR light irradiation (Fig. 2c), which might be due to blocking of the pathway to photo-byproducts under the lower energy of light irradiation.[39] As expected, a large cyclization quantum yield (φ_{o-c}) for **BFBDTE** in toluene was recorded as 0.56 and its cycloreversion quantum yield (φ_{c-o}) was 0.031. Subsequently, we further evaluated the photochromism of **BFBDTE** in $CHCl_3$ and DMSO with larger polarity. Similar photochromic behavior was observed when these three solutions were exposed to the same light conditions (Fig. S7–S10†). In contrast, the absorption maximum of the open and closed isomers showed a distinct bathochromic shift in $CHCl_3$ and DMSO (*e.g.* **BFBDTE(o):** $\lambda = 523$ nm in DMSO, $\lambda = 516$ nm in $CHCl_3$; **BFBDTE(c):** $\lambda = 758$ nm in DMSO, $\lambda = 756$ nm in $CHCl_3$) (Fig. 2d and Table S2†), indicating a unique solvent-dependent photochromic property. However, it took a longer time to reach the photostationary state in these two solvents, *i.e.*, 28 s in $CHCl_3$ and 70 s in DMSO, which implied that the higher the solvent polarity, the slower the cyclization. As expected, the corresponding cyclization quantum yields decreased as the solvent polarity increased (Table S2†). Therefore, **BFBDTE** presents exceptional photochromism triggered by green light in different solvents. Besides, the photoisomerization of **BFBDTE** was further analyzed *via* the ^{1}H NMR spectral variations in toluene-d_8 (Fig. S11†). The photocyclization conversion ratio in the photostationary state was determined to be 66.7% according to the ^{1}H NMR results.

Given the excellent photophysical properties of BF_2bdk-based complexes, the following exploration focused on the investigation of the photoluminescence (PL) performance of **BFBDTE** in solution under both prompt and delayed modes. Excited at 450 nm, **BFBDTE** exhibited bright yellow emission centered at *ca.* 556 nm in toluene. Alternatively, a new emission peak located at 572 nm was observed in the delayed mode in toluene ($\lambda_{ex} = 450$ nm) (Fig. 3a), while very weak delayed fluorescence was detected in $CHCl_3$ and DMSO (Fig. S12†). The delayed emission intensity increased with rising of the temperature from 77 to 300 K, indicating the TADF character of **BFBDTE** in toluene (Fig. 3b). Measured at 77 K, the prompt and delayed emission peaks afforded a small ΔE_{ST} of 0.09 eV between the excited S_1 (559 nm, 2.22 eV) and T_1 (582 nm, 2.13 eV) states. Upon irradiation with green light, the emission peak at 556 nm was gradually quenched (Fig. 3c) along with the fading of the yellow fluorescence in toluene (Fig. 3c insets), probably owing to efficient energy transfer between the excited BF_2bdk and closed DTE core.[40] After reaching the photostationary state in 16 s, the fluorescence intensity of **BFBDTE(o)** was quenched by *ca.* 88%. Its fluorescence returned to the original intensity after irradiation with 770 nm NIR light.

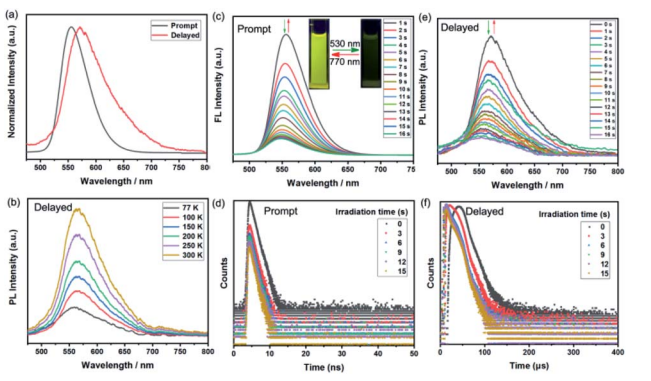

Fig. 3 (a) PL spectra of **BFBDTE** in toluene measured under prompt and delayed mode at room temperature ($\lambda_{ex} = 450$ nm). (b) Delayed fluorescence spectra of **BFBDTE** in toluene measured in the temperature range of 77 to 300 K. Prompt fluorescence spectra (c) and decay curves (d) of **BFBDTE** in toluene upon irradiation with green light (530 nm). The insets show the reversible fluorescence switching upon alternating irradiation with green and NIR (770 nm) light. Delayed fluorescence spectra (e) and decay curves (f) of **BFBDTE** in toluene upon irradiation with green light (530 nm).

Besides, this fluorescence switching process could be reversibly conducted for ten cycles with negligible degradation (Fig. S13†). Meanwhile, under the same green light irradiation, the time-resolved decay curves revealed that the prompt fluorescence lifetimes decreased from 1.73 to 1.04 ns at room temperature (Fig. 3d). Simultaneously, the TADF switching performance for **BFBDTE** was also observed in toluene. As depicted in Fig. 3e, the delayed fluorescence intensity at 572 nm was gradually decreased when exposed to green light irradiation, which in turn returned to the original intensity after irradiation with NIR light. This was accompanied by changes in the lifetimes of long-lived species from 28.57 to 13.03 μs at room temperature (Fig. 3f). Compared with that in toluene, the prompt emission peak of **BFBDTE(o)** displayed a significant red-shift in $CHCl_3$ (577 nm) and DMSO (564 nm) (Fig. S14†). Moreover, similar prompt fluorescence switch behavior was observed in $CHCl_3$ and DMSO under the same irradiation (Fig. S15 and S16, and Table S3†). To date, fluorescent photochromism materials controlled by visible light are highly desirable in both biological and materials sciences. As far as we know, the reported **BFBDTE** in our work is the first example of green-/NIR-light-controlled switching by the combination of photochromism, fluorescence and TADF with fast photoresponsive speed.

A possible photophysical process was speculated based on theoretical calculations for both **BFBDTE(o)** and **BFBDTE(c)**. In the cycloreversion state (Fig. S17†), it shows complete separation of molecular orbitals owing to the twisty conformation of **BFBDTE(o)**. The highest occupied molecular orbital (HOMO) mainly appears on the benzene ring and adjacent thiophene ring. The lowest unoccupied molecular orbital (LUMO) is exclusively located on the BF_2bdk core, double bonds and thiophene rings. Therefore, the photophysical process for **BFBDTE(o)** can be assigned to charge transfer from the DTE moiety to the BF_2bdk-based fluorophore. By contrast, the extended π-conjugated system of **BFBDTE(c)** possesses large overlap between the HOMO and LUMO (Fig. S18†). Delocalized molecular orbitals distribute on the entire cyclized molecule with a planar conformation. The extended π-conjugated system prevents the charge transfer process, leading to the quenching of the PL. Energy level (Fig. S19†) analysis shows a band gap of 2.28 eV (543 nm) for the first excited singlet state (S_1) stemmed from excitation from the HOMO to the LUMO, corresponding to the prompt emission peak at 556 nm. The energy gap (ΔE_{ST}) between S_1 and T_1 was calculated as 0.14 eV, which is very close to the experimental one (0.09 eV). Combining the experiments and theoretical calculations, it was revealed that the presence of BF_2bdk can largely reduce the energy level/gap and ΔE_{ST}, which enables the efficient energy transfer of $S_1 \rightarrow T_1$, and then, the small energy gap between BF_2bdk and DTE promotes energy transfer from T_1 of BF_2bdk to S_1 of DTE, featuring rapid photochromism performance.

Encouraged by the excellent fluorescent photochromic performance of **BFBDTE** in toluene, its photochromism and dual-mode fluorescence switching performance were further evaluated in a poly(methyl methacrylate) film (PMMA). As shown in Fig. 4a, when exposed to green light irradiation (530 nm), a novel NIR absorption band at 744 nm gradually appeared, accompanied by the film color changing from orange-red to green (Fig. 4a, insets). During this process, it took only 12 s to reach the photostationary state and 20 s for the cycloreversion reaction to return to the initial orange-red film by irradiation with NIR (770 ns). The photoresponsive speed is faster than that in polar solvents mentioned in the preceding text. In addition, good fatigue resistance was also detected under green/NIR light irradiation (Fig. S20†). As expected, **BFBDTE** presents both prompt and delayed photoluminescence in the PMMA film under excitation at 450 nm (Fig. 4b). The prompt and delayed fluorescence lifetime was estimated as 1.85 ns and 48.75 μs, respectively (Fig. S21†). As illustrated in Fig. 4c, under constant green light irradiation for 11 s, the prompt yellow emission located at 569 nm sharply decreased along with the yellow fluorescence fading in the PMMA film. Irradiation of NIR light, in turn, reverted it back to the initial intensity. Furthermore, the **BFBDTE** PMMA film also displays fast delayed switching behavior (11 s) under the same irradiation conditions (Fig. 4d). Therefore, the NIR switching of the **BFBDTE** PMMA film with a fast response rate could serve as promising for infrared wavelength detectors applied in the fields of optical communications, anti-counterfeiting, bioimaging and optical memory storage systems.

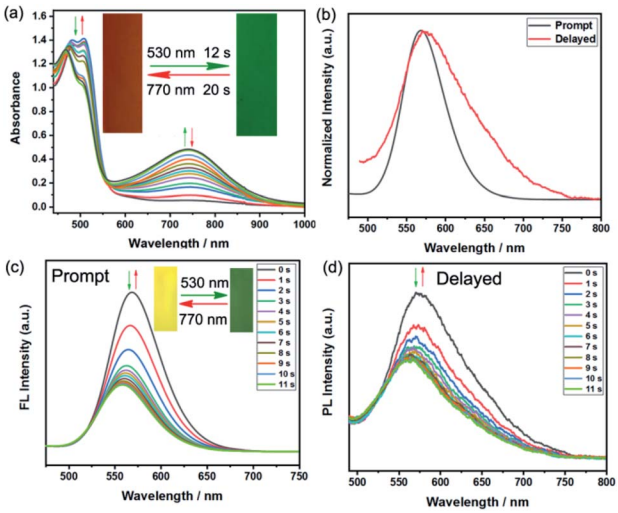

Fig. 4 (a) The absorption spectra of **BFBDTE** in the PMMA film upon alternating irradiation with green and NIR light. Inset: corresponding color changes upon light irradiation. (b) Prompt and delayed fluorescence spectra of **BFBDTE** in the PMMA film. Prompt (c) and delayed (d) fluorescence spectra of **BFBDTE** doped in the PMMA film upon alternating irradiation with green and NIR light (λ_{ex} = 450 nm). Insets: corresponding fluorescence changes upon light irradiation.

By considering the different electron structures of the **BFBDTE(o)** and **BFBDTE(c)** isomers, photo-electrochemical measurements were carried out in 0.5 M Na_2SO_4 aqueous solution with a standard three-electrode system. The working electrodes were prepared by dropping chloroform solutions of **BFBDTE(o)** and **BFBDTE(c)** onto indium tin oxide (ITO) electrodes. Ag/AgCl and platinum wire were used as the reference and counter electrodes, respectively. The cyclic voltammetry (CV) curve (Fig. 5a) shows that **BFBDTE(o)** has little electrochemical activity, whereas **BFBDTE(c)** has large electrochemical activity in the negative voltage region. A small photocurrent

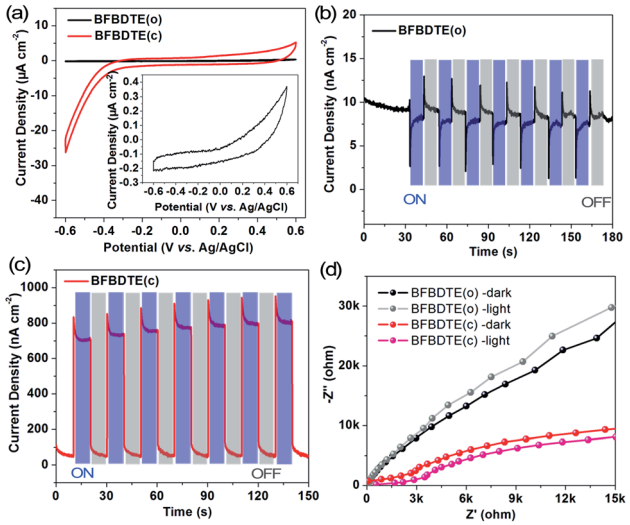

Fig. 5 (a) Cyclic voltammetry curves of **BFBDTE(o)** and **BFBDTE(c)** measured in 0.5 M Na_2SO_4 aqueous solution. Transient current density–time curves of **BFBDTE(o)** (b) and **BFBDTE(c)** (c) without bias potentials. (d) Electrochemical impedance spectroscopy (EIS) Nyquist plots of **BFBDTE(o)** and **BFBDTE(c)** measured at 0 V bias potentials.

density of only 12 nA cm^{-2} is generated for **BFBDTE(o)** under periodical on/off light irradiation without bias potential (Fig. 5b). In detail, it exhibits inverse photoelectronic response behavior: under the light-on state, the photocurrent decreases rapidly to about 2.8 nA cm^{-2} and then increases slowly to 8.3 nA cm^{-2}, while it increases rapidly and then decreases slowly when the light is turned off. By sharp contrast, **BFBDTE(c)** generates a small photocurrent density of 46 nA cm^{-2} under dark conditions, and an instantaneous increase of the photocurrent density up to 958 nA cm^{-2} is observed when the light source is turned on (Fig. 5c). Thus, under light irradiation, the photocurrent density value of **BFBDTE(c)** is 684 times higher than that of **BFBDTE(o)**. Electrochemical impedance spectroscopy (EIS) Nyquist plots (Fig. 5d) further suggest that the charge transfer resistance can be reduced under illumination for both **BFBDTE(o)** and **BFBDTE(c)**, revealing that the additional light radiation can promote the charge transfer. By contrast, **BFBDTE(c)** exhibits higher charge transfer performance than that of **BFBDTE(o)**.

The above results imply that the inefficient photoelectronic response performance of **BFBDTE(o)** can be assigned to the isolated π-conjugation localized in the two separated thiophene rings, which hinders the transport of carriers. In contrast, the extended π-conjugated system in **BFBDTE(c)** showing delocalized π-electrons can provide a charge transport channel, endowing highly efficient photoelectronic response performance. Scanning electron microscopy (SEM) images show a micrometer scale spherical morphology for both **BFBDTE(o)** and **BFBDTE(c)**. Dense aggregation microspheres with a size of about 3 μm are observed for **BFBDTE(c)**, whereas **BFBDTE(o)** exhibits a relatively sparse arrangement of microspheres with a size of about 10 μm (Fig. S22†). The reason for this morphology and arrangement diversity can be attributed to the smaller molecular size of **BFBDTE(c)** than **BFBDTE(o)** obtained from theoretical calculations (Fig. S23 and 24†). These results further demonstrate that the planar conformation of **BFBDTE(c)** with delocalized π-electrons tends to stack densely, resulting in high photoelectronic performance, which makes **BFBDTE** perfect for molecular switching controlled by NIR light.

Conclusions

In summary, a new photochromic fluorescence switching molecule, **BFBDTE**, was designed and synthesized by the conjugation of a difluoroboron β-diketonate (BF_2bdk) fluorescent unit and dithienylethene. Reversible and repeatable cyclization–cycloreversion processes can be controlled by green- and NIR-light, accompanied by a remarkable color change as well as fluorescence and TADF switching. This reversible transformation tends to the photostationary state within only 20 s in a PMMA film. We can speculate that two reasons are responsible for the above lower energy induced rapid fluorescence photochromic performance. First, the highly electrophilic boron center in BF_2bdk helps in reducing the HOMO and LUMO energy levels, as well as the energy gap, enabling the light absorption to red shift to the visible light region in the open-ring isomer. Additionally, the active nonbonding p electrons of the BF_2bdk unit favor strong spin-orbital coupling and intersystem crossing, featuring typical TADF character with small ΔE_{ST}. Second, the extended π-conjugated system in the close-ring isomer with a planar configuration further broadens the absorption band to the NIR region. The presence of electron deficient BF_2bdk, which possesses more ability to promote the homolytic bond, means that rapid cycloreversion can be realized by a lower energy of light irradiation. The delocalized π-electrons around the extended π-conjugated system in the closed-ring isomer promote charge mobility, exhibiting high electrochemical activity and photoelectronic response performance. In contrast, the open-ring isomer impedes the carrier transport, leading to turn-off of the photoelectronic response. Therefore, this study provides a new perspective into the future design of visible light-/NIR-controlled photochromic materials showing reversible TADF and photoelectronic switching.

Data availability

All of data associated with this article are presented in the manuscript and ESI.†

Author contributions

Z. Li, S. Yang, S. Chen and H. Zhou synthesized the complex. J. Zhang and X. Tian determined the single-crystal structure. S. Yang, S. Chen, H. Zhou, J. Zhang and X. Tian performed the characterization of the complex. Z. Li and X.-G. Yang designed and directed the studies and wrote the manuscript. All of the authors discussed the results and reviewed the manuscript.

Conflicts of interest

There are no conflicts to declare.

Acknowledgements

This work was supported by the National Natural Science Foundation of China (No. 21971100), the Natural Science Foundation of Henan Province (No. 222300420501), the Science and Technology Project of Henan Province (No. 212102210549), the Key Scientific Research Project of Higher Education of Henan Province (No. 22A430007), and the Innovation and Entrepreneurship Training Program for College students in China (No. 202110482010).

Notes and references

1 (*a*) K. Uno, A. Aktalay, M. L. Bossi, M. Iriec, V. N. Belov and S. W. Hell, *Proc. Natl. Acad. Sci. U.S.A.*, 2021, **118**, e2100165118; (*b*) H.-B. Cheng, S. Zhang, E. Bai, X. Cao, J. Wang, J. Qi, J. Liu, J. Zhao, L. Zhang and J. Yoon, *Adv. Mater.*, 2022, **34**, 2108289.
2 N. M.-W. Wu, M. Ng and V. W.-W. Yam, *Nat. Commun.*, 2022, **13**, 33.
3 L. Kortekaas and W. R. Browne, *Chem. Soc. Rev.*, 2019, **48**, 3406–3424.
4 D. Kim, K. Jeong, J. E. Kwon, H. Park, S. Lee, S. Kim and S. Y. Park, *Nat. Commun.*, 2019, **10**, 3089.
5 R. Usui, K. Yamamoto, H. Okajima, K. Mutoh, A. Sakamoto, J. Abe and Y. Kobayashi, *J. Am. Chem. Soc.*, 2020, **142**, 10132–10142.
6 H. Yang, M. Li, C. Li, Q. Luo, M.-Q. Zhu, H. Tian and W.-H. Zhu, *Angew. Chem., Int. Ed.*, 2020, **59**, 8560–8570.
7 M. Irie, T. Fukaminato, K. Matsuda and S. Kobatake, *Chem. Rev.*, 2014, **114**, 12174–12277.
8 Y. Mu, Y. Liu, H. Tian, D. Ou, L. Gong, J. Zhao, Y. Zhang, Y. Huo, Z. Yang and Z. Chi, *Angew. Chem., Int. Ed.*, 2021, **60**, 6367–6371.
9 R. Haldar, L. Heinke and C. Wöll, *Adv. Mater.*, 2019, 1905227.
10 E. C. Harvey, B. L. Feringa, J. G. Vos, W. R. Browne and M. T. Pryce, *Coord. Chem. Rev.*, 2015, **282–283**, 77–86.
11 (*a*) Y. Qin, Y.-T. Wang, H.-B. Yang and W. Zhu, *Chem. Synth.*, 2021, **1**, 2; (*b*) G. Naren, W. Larsson, C. Benitez-Martin, S. Li, E. P. Inestrosa, B. Albinsson and J. Andreasson, *Chem. Sci.*, 2021, **12**, 7073–7078.
12 K. E. Sapsford, L. Berti and I. L. Medintz, *Angew. Chem., Int. Ed.*, 2006, **45**, 4562–4588.
13 T. Fukaminato, T. Doi, N. Tamaoki, K. Okuno, Y. Ishibashi, H. Miyasaka and M. Irie, *J. Am. Chem. Soc.*, 2011, **133**, 4984–4990.
14 K. Uno, H. Niikura, M. Morimoto, Y. Ishibashi, H. Miyasaka and M. Irie, *J. Am. Chem. Soc.*, 2011, **133**, 13558–13564.
15 A. Nagai, R. Nishimura, Y. Hattori, E. Hatano, A. Fujimoto, M. Morimoto, N. Yasuda, K. Kamada, H. Sotome, H. Miyasaka, S. Yokojima, S. Nakamura and K. Uchida, *Chem. Sci.*, 2021, **12**, 11585–11592.
16 C. Li, H. Yan, L.-X. Zhao, G.-F. Zhang, Z. Hu, Z.-L. Huang and M.-Q. Zhu, *Nat. Commun.*, 2014, **5**, 5709.
17 J.-X. Liu, B. Xin, C. Li, N.-H. Xie, W.-L. Gong, Z.-L. Huang and M.-Q. Zhu, *ACS Appl. Mater. Interfaces*, 2017, **9**, 10338–10343.
18 A. Nagai, R. Nishimura, Y. Hattori, E. Hatano, A. Fujimoto, M. Morimoto, N. Yasuda, K. Kamada, H. Sotome, H. Miyasaka, S. Yokojima, S. Nakamura and K. Uchida, *Chem. Sci.*, 2021, **12**, 11585–11592.
19 C. Li, K. Xiong, Y. Chen, C. Fan, Y.-L. Wang, H. Ye and M.-Q. Zhu, *ACS Appl. Mater. Interfaces*, 2020, **12**, 27651–27662.
20 Z. Li, Y. Pei, Y. Wang, Z. Lu, Y. Dai, Y. Duan, Y. Ma and H. Guo, *J. Org. Chem.*, 2019, **84**, 13364–13373.
21 Z. Li, Y. Dai, Z. Lu, Y. Pei, H. Chen, L. Zhang, Y. Duan and H. Guo, *Chem. Commun.*, 2019, **55**, 13430–13433.
22 T. Fukaminato, T. Hirose, T. Doi, M. Hazama, K. Matsuda and M. Irie, *J. Am. Chem. Soc.*, 2014, **136**, 17145–17154.
23 W. Tan, J. Zhou, F. Li, T. Yi and H. Tian, *Chem. - Asian J.*, 2011, **6**, 1263–1268.
24 T. Sumi, T. Kaburagi, M. Morimoto, K. Une, H. Sotome, S. Ito, H. Miyasaka and M. Irie, *Org. Lett.*, 2015, **17**, 4802–4805.
25 B. Seefeldt, K. Altenhöner, O. Tosic, T. Geisler, M. Sauer and J. Mattay, *Photochem. Photobiol. Sci.*, 2011, **10**, 1488–1495.
26 H. Uoyama, K. Goushi, K. Shizu, H. Nomura and C. Adachi, *Nature*, 2012, **492**, 234–238.
27 Y. Tao, K. Yuan, T. Chen, P. Xu, H. Li, R. Chen, C. Zheng, L. Zhang and W. Huang, *Adv. Mater.*, 2014, **26**, 7931–7958.
28 Z. Yang, Z. Mao, Z. Xie, Y. Zhang, S. Liu, J. Zhao, J. Xu, Z. Chi and M. P. Aldred, *Chem. Soc. Rev.*, 2017, **46**, 915–1016.
29 V.-N. Nguyen, A. Kumar, M. H. Lee and J. Yoon, *Coord. Chem. Rev.*, 2020, **425**, 213545.
30 W. Chen and F. Song, *Chin. Chem. Lett.*, 2019, **30**, 1717–1730.
31 Z. Yang, Z. Mao, Z. Xie, Y. Zhang, S. Liu, J. Zhao, J. Xu, Z. Chi and M. P. Aldred, *Chem. Soc. Rev.*, 2017, **46**, 915–1016.
32 C. Wang and Y. Liu, *Mater. Today Chem.*, 2022, **25**, 100954.
33 Y. Xie, Y. Ge, Q. Peng, C. Li, Q. Li and Z. Li, *Adv. Mater.*, 2017, **29**, 1606829.
34 F. B. Dias, K. N. Bourdakos, V. Jankus, K. C. Moss, K. T. Kamtekar, V. Bhalla, J. Santos, M. R. Bryce and A. P. Monkman, *Adv. Mater.*, 2013, **25**, 3707–3714.
35 (*a*) C.-T. Poon, W. H. Lam, H.-L. Wong and V. W.-W. Yam, *J. Am. Chem. Soc.*, 2010, **132**, 13992–13993; (*b*) C. C.-T. Poon, W. H. Lam and V. W.-W. Yam, *Chem. - Eur. J.*, 2013, **19**, 3467–3476; (*c*) C.-L. Wong, C.-T. Poon and V. W.-W. Yam, *Chem. - Eur. J.*, 2016, **22**, 12931–12940.
36 (*a*) M. Morimoto, H. Miyasaka, M. Yamashita and M. Irie, *J. Am. Chem. Soc.*, 2009, **131**, 9823–9835; (*b*) V. Ramamurthy and K. Venkatesan, *Chem. Rev.*, 1987, **87**, 433–481.
37 X. Ma, W. Chi, X. Han, C. Wang, S. H. Liu, X. Liu and J. Yin, *Chin. Chem. Lett.*, 2021, **32**, 1790–1794.
38 (*a*) Y. Qin, L.-J. Chen, Y. Zhang, Y.-X. Hu, W.-L. Jiang, G.-Q. Yin, H. Tan, X. Li, L. Xu and H.-B. Yang, *Chem. Commun.*, 2019, **55**, 11119–11122; (*b*) J. Xu, H. Volfova, R. J. Mulder, L. Goerigk, G. Bryant, E. Riedle and C. Ritchie, *J. Am. Chem. Soc.*, 2018, **140**, 10482–10487.
39 M. Herder, B. M. Schmidt, L. Grubert, M. Patzel, J. Schwarz and S. Hecht, *J. Am. Chem. Soc.*, 2015, **137**, 2738–2747.
40 T. Kawai, T. Sasaki and M. Irie, *Chem. Commun.*, 2001, 711–712.